The corrosion protection ability of TiAlN coatings produced with CA-PVD under superimposed pulse bias

Er, D, Taghavi Pourian Azar, G, Kazmanlı, K & Urgen, M

DOI 10.1016/j.surfcoat.2018.04.034
ISSN 0257-8972
ESSN 1879-3347
Publisher: Elsevier

THE CORROSION PROTECTION ABILITY OF TiAlN COATINGS PRODUCED WITH CA-PVD UNDER SUPERIMPOSED PULSE BIAS

Dilan Er[1], Golnaz Taghavi Pourian Azar[1], Kürşat Kazmanlı[1]and Mustafa Ürgen[1*]

[1]Istanbul Technical University, Department of Metallurgical and Materials Engineering, 34469, Maslak, Istanbul, Turkey

Abstract

In this study we have investigated the contribution of superimposing high voltage pulse on DC bias on the corrosion protection ability of TiAlN coatings deposited with cathodic arc physical vapor deposition (CA-PVD). Superimposing high voltage on DC bias resulted in the decrease of the number of attached macroparticles (MP) and also densified the columnar structure. These differences significantly improved the corrosion protection ability of the coatings that were determined by electrochemical impedance spectroscopy (EIS) in 0.1 N HCl solutions. An approximately 6 fold increase in the polarization resistance for the samples deposited by using -1000 V superimposed pulse voltage on 40 V DC bias when compared to the ones deposited only by DC bias. For further elaborating these results, the distribution, size and morphology of the corrosion sites were determined with ferroxyl test, scanning electron microscopy (SEM) and 3D optical profilometry. Results of the ferroxyl tests indicated a dramatic decrease of corrosion sites by superimposing -1000 V on DC bias. Closer investigation of these sites showed that corrosion of the substrate is first initiated at the bottom of the defects extending through the coating and then expanded below the coating. The depths and diameters of the corroding sites, revealed by removing their caps with ultrasonication were substantially lower for the samples produced with superimposed bias. Results of the study indicated the necessity of combining electrochemical corrosion test results with the morphology and distribution of corrosion sites for a proper understanding of the corrosion protection ability of hard coatings.

Key words: CA-PVD; Superimposed pulse bias; TiAlN coatings; Corrosion; EIS; Ferroxyl test.

1. INTRODUCTION

Nitride based hard ceramic coatings especially TiN, CrN and TiAlN are highly demanded for tribological applications owing to their superior hardness and tribological properties. Application areas of nitride based hard ceramic coatings are not only limited to tribological practices but also to corrosion protection, decorative coatings, electrical circuit elements, etc. because of their high oxidation resistance, appeal and good electrical conductivity [1-5].

High corrosion resistance of nitride based hard ceramic coatings has drawn a significant attention for utilization of them as corrosion protective coatings. Many studies have been performed with different coatings in various medias to investigate the corrosion behavior of nitride based hard ceramic coatings and these efforts have been reviewed by Jehn et al. [3] and recently by Fenker et al [5]. According to these studies, hard ceramic coatings deposited on inert substrates show almost excellent corrosion resistance. However, poor corrosion protection ability was obtained from hard coatings deposited on low corrosion resistant substrates [6-8]. This behavior is related to the defects extending through the coatings to the substrates [6]. Hard ceramic coatings produced by PVD have columnar structure and some inherent defects, such as porosities, voids, pinholes, and macro droplets (MP) in the case of cathodic arc physical vapor deposition (CA-PVD) [1-6]; [9 -11]. These defects and columnar structure is the main drawback of hard coatings that limit their usage for corrosion protection [5]. Different strategies and approaches have been used to improve corrosion protection ability of ceramic hard coatings such as optimization of coating parameters, multilayer coatings, composite and nano-composite coating applications, increasing coating thickness, and deposition of a metallic interlayer between the substrate and coating [12-19].

Among these nitride based hard ceramic coatings, TiAlN is known to exhibit comparably better corrosion protection ability, which is attributed to the self-repairing properties owing to the presence of Al in their structure [20]. There are many studies focused on the investigation of corrosion behavior of TiAlN coatings, which are deposited on different substrates and tested in different aggressive media. According to these works, TiAlN coatings considerably enhance the corrosion resistance of the system in most of the corrosive environments [20-22]. On the other hand, the corrosion protection ability of TiAlN coatings can be lower than expected and not always be highest compared to the other nitride based hard ceramic coatings depending on the substrate material, corrosive media and the structural properties of the coating [18, 23, 24].

In this work we aimed to investigate the structural and morphological effects induced by superimposing high voltage pulse on DC bias on the corrosion protective properties of TiAlN coatings. In our previous work [25], we have observed that this mode of bias application resulted in a significant decrease in macro particle attachment and densified the columnar structure. Both of these modifications are expected to exert positive influence on corrosion protection ability of the coatings by reducing the defects, pinholes extending through the coating to the substrate. For achieving this aim, we investigated the time dependent corrosion behavior of the coated samples with electrochemical impedance spectroscopy (EIS) analysis. For further evaluating the corrosion protection ability of the coatings, ferroxyl test was applied to the samples that were subjected to the corrosion tests. SEM and optical profilometry studies are conducted on active corroding sites that were marked by ferroxyl test for the determination of corroding site morphology and distribution.

2. EXPERIMENTAL STUDIES

TiAlN coatings were deposited on metallographically mirror polished low carbon steel (AISI 1010) substrates having 2.5 x 5 x 0.3 cm dimensions. Prior to the deposition process, samples were cleaned ultrasonically in alkaline solution for 15 min and in ethanol for 10 min, respectively. Then, the samples were cleaned with distilled water, dried with ethanol, and placed into the vacuum chamber. Coating procedure was carried out in a Novatech-SIE, Model: NVT-12 cathodic arc physical vapor deposition (CA-PVD) unit. Sample surfaces were ion etched using Ti ion plasma under -1000 V pulse bias with a duty cycle of 80 % for a duration of 4 min. After that, Ti and TiN interlayers were deposited by applying -150 V DC bias voltage each for 1 min. TiAlN coatings were realized by using Ti-Al (50:50) cathode under DC and superimposed pulse bias modes in 2.5 Pa nitrogen atmosphere using a DC bias magnitude of -40 V for a duration of 30 min. 500 and 1000 V superimposed pulse bias magnitudes were used in the study. Both Ti and TiAl cathodes were operated at 60 A. Details of the coating parameters were presented in Table 1.

The corrosion behavior of TiAlN coatings was investigated by using electrochemical impedance spectroscopy (EIS) (Bio Logic, Model SP-150 potentiostat/galvanostat) in deaerated 0.1 N HCl (pH =1) solution at room temperature. Before the tests, carbon steel substrate and coated samples were ultrasonically cleaned in ethanol-acetone solution for 10 min, then cleaned with distilled water and dried with ethanol. The samples were masked by applying chemical resistant epoxy resin

(Duratek - AV 80), for exposing specifically determined open area to the solution. Electrochemical tests were conducted in a 3-electrode cell, using steel substrate and coated samples as working electrode, Ag/AgCl reference electrode, and rod shaped graphite as counter electrode. Before the engagement of the samples, HCl solution was purged with nitrogen gas for 20 min to eliminate dissolved oxygen in the system, then samples were immersed into the solution and purging process was continued during the test. EIS measurements were carried out at open circuit potential (corrosion potential), between 10 mHz - 45 kHz frequency range with 10 mV amplitude. These measurements were repeated successively to obtain time dependent AC impedance data of the samples. Total duration of the electrochemical tests was 5 h. Surface morphology of the corroded samples was investigated using SEM (JEOL JSM 5410). In order to supplement the corrosion test results, ferroxyl test was applied (in accordance to ISO 10309 standard) [26] to the coated samples that were subjected to the electrochemical tests for 5 h. Afterwards samples were placed into the ultrasonic system (SONICS Vibra Cell) for 1 min to open the top of the corroded sites and reveal the exact corroding area of the steel substrate. Samples were further investigated via optical profiling system (Veeco, Model: WYKO NT1100) to obtain 2D and 3D images of the pits.

3. Results and discussion

3.1 Structural and morphological investigations of the coatings

The details of modifications on the morphology and structural properties of TiAlN coatings depending on different bias mode applications (DC and superimposed bias modes) were given in our previous study [25]. According to the results of this study, application of superimposed bias on DC decreased the amount of macro particles (MPs) on TiAlN coatings remarkably (Fig. 1). Several mechanisms have been proposed for the explanation of the decrease of macro particle attachment with the use of high voltage biasing, including enhanced ion sputtering of the protruding MPs [27], removal of loosely bonded MPs due to the incident high energy ions [28, 29], evaporation of MPs in the sheath as a result of their collision with the high energy ions [30] and reflection of them by the sheath electric field [31, 32] repeated negative charging of MPs due to the oscillations of plasma sheath thickness under pulsed bias, contrary to the stable plasma sheath thickness in the case of DC bias [33].

Another effect induced by high energy pulses of bias is the densification of grain boundaries by the increase of ad atom mobility [34], that is reflected to the microstructure as dense fine columnar structure [25].

3.2 Time dependent polarization resistance of the samples

For the determination of time dependent corrosion resistance of the samples, EIS measurements were performed and polarization resistance (R_p) were obtained from Nyquist plots. Corrosion rate and Rp are inversely related to each other according to the Stern-Geary equation [35-37],

$$i_{corr} = \frac{k}{R_P} \quad (1)$$

where i_{corr} is the corrosion current density, i.e. corrosion rate, R_p is polarization resistance, and k is a constant, which includes anodic and cathodic Tafel slopes.

Rp values extracted from Nyquist plots indicate better corrosion behavior of the coated samples (Table 2). R_p of all samples decreased with increasing immersion time. This expected downward trend of R_p is the result of prolonged uniform corrosion phenomena in mild steel substrate and extension of localized corrosion in the substrates below the defects, i.e. porosities [6, 37-39]. Even though, R_p decrease with increasing immersion time, TiAlN coatings produced by superimposed bias preserve their higher R_p when compared to steel substrate and TiAlN coated substrate produced with DC bias.

3.3 Equivalent circuit fitting of the samples

Nyquist plots of the samples obtained after 5 h exposure period are used for equivalent circuit determination and fitting process (Fig. 2). We used $R_s(Q_{dl}[R_p])$ model for mild steel substrate (Fig. 3a) and $R_s(Q_{coat}[R_{pore}(Q_{dl}[R_p])])$ for TiAlN coatings (Fig. 3b), which are the most common equivalent circuits in the literature for steel substrate and porous electrodes [37, 39, 40]. In the generalized model for mild steel substrate, R_s indicates solution resistance, Q_{dl} shows capacitance of double layer and R_p (or R_{ct}) stands for polarization resistance of the substrate. In the modeled equivalent circuit for TiAlN coatings, additional circuit elements are adapted to the system as Q_{coat}, which represents the capacitance of coating and R_{pore} (charge transfer resistance of pores), besides R_p (R_{ct}) stands for polarization resistance of the coating. Constant phase element (CPE) was used instead of pure capacitance (C) in the equivalent circuits since better fitting results were obtained when C was replaced with Q. Altering perfect capacitor (C) with constant phase element (Q) in equivalent circuits is generally necessary for porous PVD coatings because of the deviation from ideal capacitor to non-ideal, i.e. leaky capacitor, that is generally associated with the surface roughness and inhomogeneity [37-41]. This deviation from the perfect capacitor can be

demonstrated by the parameter n. The n parameter varies between 0 (pure resistance) to 1 (pure capacitance) [38-41]. Thus, if n is close to 1, sample demonstrates nearly perfect capacitive character. Zsim software (Ec-Lab V 11.17) was used for fitting procedure and relative error of fitting is under 5 % for all samples.

From the fitting data given in Table 3, solution resistances were very close to each other for both uncoated and coated samples. On the other hand, Q_{dl} and n_{dl} were lower for TiAlN coated samples. However, n_{dl} values of the samples did not show a significant variation, indicating that the electrochemical character of double layer is similar for all samples.

Polarization resistance (R_p) of the samples displayed differences as expected and the results are very close to the polarization resistances obtained after 5 h exposure (Table 2). Accordingly, the highest R_p belongs to the DP1000 coating, while mild steel substrate has the lowest polarization resistance.

Pore resistance (R_{pore}) of the coated samples increased in the following order: DC, DP500 and DP1000. Liu et. al proposed that R_{pore} parameter and porosity amount are inversely proportional to each other, thus a higher R_{pore} indicates lower porosity in the coating [42].

Coating capacitor (Q_{coat}) showed a downward trend for superimposed coatings compared to DC biased TiAlN coating. This behavior could be attributed to the lower porosity amount in the coatings produced by superimposed biasing [39]. In addition, n_{coat} of the DP samples were very close to 1 indicating their almost perfect capacitor behavior.

These results showed the higher corrosion protection ability of TiAlN coatings produced with superimposed bias. However, these results do not include the morphological features of corrosion damage such as corroded site size, distribution and morphology. In the next sections, results on the size and distribution of the corroded sites that were examined by ferroxyl test, SEM and optical profilometry were presented.

3.4 Distribution, size and morphology of the corrosion sites on the coated samples

For the visual determination of the corrosion sites on the coated samples, which were exposed, to the corrosion test for 5 h., ferroxyl test were performed. From the macro images of TiAlN coatings, it was clearly observed that DC coating has the highest number of corrosion sites, i.e. marked as blue spots (Fig. 4a), that decreased substantially in the case of the sample produced with

superimposing -1000 V pulse on DC bias (DP1000 sample) (Fig. 4c). The number of the blue colored corrosion sites in the coatings was given in Table 4. These results are partly in accordance with the results of electrochemical tests. According to the electrochemical tests the corroding area of the DC coated sample should be higher than the marked areas because Rp of this sample became very close to the Rp of the uncoated steel substrate after 5 h exposure to the corrosive medium (Table 2). On the other hand, although the marked corrosion sites of DP500 sample is close to DC sample, Rp of DP500 is almost two fold higher than DC sample.

To clarify these differences, corrosion sites marked by ferroxyl tests are investigated in detail with SEM. General character of the corrosion sites revealed that corrosion of the steel substrate under the coating started by the penetration of the solution through a defect (such as pinhole, periphery of a MP) that extends in the substrate (Fig. 5). As a result, corrosion of the substrate starts and expands inwards under the cover of the TiAlN coating. Slightly observable circular trace around the pit highly probably indicates the substrate area subjected to corrosion. As explained in the experimental section, to reveal the exact area of the corroded sites, samples were subjected to ultra-sonication to remove the coating layer above them and then investigated using SEM (Fig. 6).

SEM images of TiAlN coatings clearly showed that pits have similar morphology in all coated samples, which are spherical and have crystallographic etching appearance resulting from acidic character of the medium (Fig. 6). Diameter of the pits for DC, DP500 and DP1000 were about 50, 35 and 30 µm, respectively. In the DC and DP500 samples, around the deep pit, a shallower corrosion region that mainly extends in one direction is observed. This observation indicated the deepening of the corrosion region below the pinhole and undermining of the substrate around the periphery of the pits took place concurrently. Directionality of this expansion can be related to the position of the sample in the solution. Arrows on the figures indicate the direction of the pit expansion, i.e. hanging direction of the samples. It is well known that pits preferentially grow in the direction of gravity [43].

For determining the depth of the corroded areas after stripping their caps, optical profilometry images of the samples were taken in an area of 9 mm^2 (Fig. 7). As it can be seen from the images, there is no significant difference between the number of corroded sites for DC and DP500 coatings, while DP1000 has a few of them. On the other hand, the depths of the corroded sites showed great variations from -5 to -40 µm. The deeper corroded sites were observed in DC sample and the depths

of them decreased for the coatings produced by superimposed bias mode, being shallowest for the DP1000 sample. These results clearly indicated that for the coatings produced by superimposing pulse bias, the defect sites that lead to corrosion and their depths are decreasing by the increased magnitude of pulse bias voltage. Additionally, these results gave an insight for a proper interrelation between the electrochemical corrosion testing results and the morphological features of the corroded sites. Although the number of corroded sites in DC and DP500 samples are similar, the corrosion rates calculated from EIS measurements has an almost two fold difference (Table 2). Results of the morphological investigations after removal of the caps of corroded sites showed that this difference arouse from the corroding area of these two samples. The depths of corroded sites on DP500 samples are significantly shallower showing the important contribution of the corroding area under the coating cap in EIS measurements.

4. CONCLUSIONS

The results of this study showed that by superimposing high voltage pulse on DC bias, corrosion protection ability of TiAlN coated steels could be increased substantially. This improvement is related to the decrease in the number of MP and densification of the coating structure by superimposing high voltage bias both of which may act as the source of defects extending through the coating to the substrate**.** By increasing the magnitude of superimposed voltage to -1000 V protection ability of the coatings became more pronounced. Another outcome of this study is the necessity of combining electrochemical corrosion test results with the morphology and distribution of corrosion sites. For a proper interpretation of corrosion protective properties of the coatings, electrochemical test results and the real area of the corroding sites on the substrate should be determined because during electrochemical tests total area of corroding substrate is the main determining parameter of the corrosion rate (Rp). In our case we have determined that corrosion of the substrate that initiates at a defect site extending through the coating continues to grow below TiAlN coating layer. The removal of the coating layer above the corroding site revealed the real working area of corrosion. The depths and diameters of the corroded sites on the substrates decreased in the following order DC- DP500 and DP1000.

Acknowledgments

This work has been supported within the scope of the bilateral project between The National Academy of Science of Ukraine (NASU) and the Scientific and Technological Research Council of Turkey (TUBITAK) (Contract No. 114M554).

REFERENCES

[1] H. Calışkan, P. Panjan, C. Kurbanoğlu, Hard Coatings on Cutting Tools and Surface Finish, in: S. Hashmi (Ed.), Compr. Mater. Finish., Elsevier Ltd., 2017: pp. 230–242. doi:10.1016/B978-0-12-803581-8.09178-5.

[2] A.K. Krella, Degradation of Protective PVD Coatings, in: A.S.H. Makhlouf, M. Aliofkhazraei (Eds.), Handb. Mater. Fail. Anal. with Case Stud. from Chem. Concr. Power Ind., 2016: pp. 411–440. doi: 10.1016/B978-0-08-100116-5.00016-8.

[3] H.A. Jehn, M.E. Baumgärtner, Corrosion studies with hard coating-substrate systems, Surf. Coatings Technol. 54–55 (1992) 108–114. doi:10.1016/S0257-8972(09)90036-6.

[4] M. Ürgen, A.F. Çakır, The effect of heating on corrosion behavior of TiN- and CrN-coated steels, Surf. Coatings Technol. 96 (1997) 236–244. doi:10.1016/S0257-8972(97)00123-0.

[5] M. Fenker, M. Balzer, H. Kappl, Corrosion protection with hard coatings on steel : Past approaches and current research efforts, Surf. Coat. Technol. 257 (2014) 182–205. doi:10.1016/j.surfcoat.2014.08.069.

[6] B. Elsener, A. Rota, H. Böhni, Impedance study on the corrosion of PVD and CVD titanium nitride coatings, Mater. Sci. Forum. 44–45 (1989) 29–38. doi:10.4028/www.scientific.net/MSF.44-45.29.

[7] M. Tavi, O. Forsén, J. Aromaa, Corrosion testing of ZrN and TiN films, Mater. Sci. Forum. 44–45 (1989) 15–28. doi:10.4028/www.scientific.net/MSF.44-45.15.

[8] Y. Massiani, A. Medjahed, P. Gravier, J.P. Crousier, Effect of a titanium underlayer on the corrosion behaviour of physically vapour deposited titanium nitride films, Thin Solid Films. 217 (1992) 31–37. doi:https://doi.org/10.1016/0040-6090(92)90602-8.

[9] A. Anders, Cathodic Arcs: From Fractal Spots to Energetic Condensation, Springer, New York, 2008. doi: 10.1007/978-0-387-79108-1.

[10] A. Anders, Unfiltered and Filtered Cathodic Arc Deposition, in: P.M. Martin (Ed.), Handb. Depos. Technol. Film. Coatings, 3rd ed., Elsevier, 2010, pp. 466–531. doi:10.1016/B978-0-8155-2031-3.00010-7.

[11] J. Koskinen, Cathodic-Arc and Thermal-Evaporation Deposition, in: S. Hashmi (Ed.), Compr. Mater. Process., 2014: pp. 3–55. doi: 10.1016/B978-0-08-096532-1.00409-X.

[12] W. Yongqiang, C. Xiaoxia, T. Xiubo, G. Chunzhi, Y. Shiqin, J. Zhiqiang, C. Liangji, Effects of pulsed bias duty ratio on microstructure and surface properties of TiN films, Vacuum. 89 (2013) 185–189. doi: 10.1016/j.vacuum.2012.04.016.

[13] M. Flores, L. Huerta, R. Escamilla, E. Andrade, S. Muhl, Effect of substrate bias voltage on corrosion of TiN/Ti multilayers deposited by magnetron sputtering, Appl. Surf. Sci. 253 (2007) 7192–7196. doi:10.1016/j.apsusc.2007.02.203.

[14] D. V Tzaneva, V.I. Dimitrova, P.E. Hovsepyan, Influence of the formation conditions of TiN coatings on their electrochemical behaviour in sulphuric acid and sodium chloride solutions, Thin Solid Films. 295 (1997) 178–184. doi: 10.1016/S0040-6090(96)09207-3.

[15] M.J. Park, A. Leyland, A. Matthews, Corrosion performance of layered coatings produced by physical vapour depostion, Surf. Coatings Technol. 43–44 (1990) 481–492. doi: 10.1016/0257-8972(90)90099-X.

[16] K. Shukla, R. Rane, J. Alphonsa, P. Maity, S. Mukherjee, Structural, mechanical and corrosion resistance properties of Ti/TiN bilayers deposited by magnetron sputtering on AISI 316L, Surf. Coat. Technol. 324 (2017) 167–174. doi: 10.1016/j.surfcoat.2017.05.075.

[17] P.M. Perillo, Corrosion behavior of coatings of titanium nitride and titanium-titanium nitride on steel substrates, Corrosion. 62 (2006) 182–185. doi:10.5006/1.3278263.

[18] M. A. M. Ibrahim, S.F. Korablov, M. Yoshimura, Corrosion of stainless steel coated with TiN, (TiAl) N and CrN in aqueous environments, Corros. Sci. 44 (2002) 815–828. doi:10.1016/S0010-938X(01)00102-0.

[19] H.A. Jehn, Improvement of the corrosion resistance of PVD hard coating-substrate systems, Surf. Coatings Technol. 125 (2000) 212–217. doi:10.1016/S0257-8972(99)00551-4.

[20] Y. Li, L. Qu, F. Wang, The electrochemical corrosion behavior of TiN and (Ti,Al)N coatings in acid and salt solution, Corros. Sci. 45 (2003) 1367–1381. doi:10.1016/S0010-938X(02)00223-8.

[21] R. Ananthakumar, B. Subramanian, A. Kobayashi, M. Jayachandran, Electrochemical corrosion and materials properties of reactively sputtered TiN/TiAlN multilayer coatings, Ceram. Int. 38 (2012) 477–485. doi:10.1016/j.ceramint.2011.07.030.

[22] Y.H. Yoo, D.P. Le, J.G. Kim, S.K. Kim, P. Van Vinh, Corrosion behavior of TiN, TiAlN, TiAlSiN thin films deposited on tool steel in the 3.5 wt.% NaCl solution, Thin Solid Films. 516 (2008) 3544–3548. doi:10.1016/j.tsf.2007.08.069.

[23] L. Cunha, M. Andritschky, L. Rebouta, R. Silva, Corrosion of TiN, (TiAl)N and CrN hard coatings produced by magnetron sputtering, Thin Solid Films. 317 (1998) 351–355. doi:10.1016/S0040-6090(97)00624-X.

[24] R.M. Souto, H. Alanyali, Electrochemical characteristics of steel coated with TiN and TiA1N coatings, Corros. Sci. 42 (2000) 2201–2211. doi:10.1016/S0010-938X(00)00057-3.

[25] G. Taghavi Pourian Azar, D. Er, M. Urgen, The role of superimposing pulse bias voltage on DC bias on the macroparticle attachment and structure of TiAlN coatings produced with CA-PVD, Surf. Coatings Technol. (2018), https://doi.org/10.1016/j.surfcoat.2018.02.066

[26] ISO 10309 (1994). Metallic Coatings-Porosity Tests-Ferroxyl Test.

[27] R.R. Aharonov, M. Chhowalla, S. Dhar, R.P. Fontana, Factors affecting growth defect formation in cathodic arc evaporated coatings, Surf. Coat. Technol. 82 (1996) 334-343.

[28] M. Li, F. Wang, Effects of nitrogen partial pressure and pulse bias voltage on (Ti,Al)N coatings by arc ion plating, Surf. Coat. Technol. 167 (2003) 197-202.

[29] W. Olbrich, J. Fessmann, G. Kampschulte, Improved control of TiN coating properties using cathodic arc evaporation with a pulsed bias, Surf. Coat. Technol. 49 (1991) 258-262.

[30] A.N. Kale, K. Ravindranath, D.C. Kothari, P.M. Raole, Tribological properties of (Ti,Al) N coatings deposited at different bias voltages using the cathodic arc technique, Surf. Coat. Technol. 145 (2001) 60-70.

[31] A.I. Ryabchikov, D.O. Sivin, A.I. Bumagina, Physical mechanisms of macroparticles number density decreasing on a substrate immersed in vacuum arc plasma at negative high-frequency short-pulsed biasing, Appl. Surf. Sci. 305 (2014) 487-491.

[32] A.I. Ryabchikov, P.S. Ananin, D.O. Sivin, S.V. Dektyarev, A.I. Bumagina, A.E. Shevelev, D.A. Andriyashin, Influence of negative bias pulse parameters on accumulation of macroparticles on the substrate immersed in titanium vacuum arc plasma, Surf. Coat. Technol. 306 (2016) 251-256.

[33] M. Huang, G. Lin, Y. Zhao, Ch. Sun, L. Wen, Ch. Dong, Macro-particle reduction mechanism in biased arc ion plating of TiN, Surf. Coat. Technol. 176 (2003) 109-114.

[34] D. Magnfalt, G. Abadias, K. Sarakinos, Atom insertion into grain boundaries and stress generation in physically vapor deposited films, Appl. Phys. Lett. 103, 051910 (2013); doi: 10.1063/1.4817669.

[35] M. Stern, A.L. Geary, Electrochemical Polarization, J. Electrochem. Soc. 104 (1957) 56-63. doi:10.1149/1.2428496.

[36] E. Barsoukov, J.R. Macdonald, eds., Impedance spectroscopy: theory, experiment, and applications, Jonh Wiley & Sons, 2005. ISBN: 978-0-471-64749-2.

[37] C. Liu, A. Leyland, S. Lyon, A. Matthews, Electrochemical impedance spectroscopy of PVD-TiN coatings on mild steel and AISI316 substrates, Surf. Coatings Technol. 76–77 (1995) 615–622. doi:10.1016/0257-8972(95)02545-6.

[38] C. Liu, Q. Bi, A. Leyland, A. Matthews, An electrochemical impedance spectroscopy study of the corrosion behaviour of PVD coated steels in 0.5 N NaCl aqueous solution: Part I.: Establishment of equivalent circuits for EIS data modelling, Corros. Sci. 45 (2003) 1243–1256. doi: 10.1016/S0010-938X(02)00213-5.

[39] C. Liu, Q. Bi, A. Matthews, EIS comparison on corrosion performance of PVD TiN and CrN coated mild steel in 0.5 N NaCl aqueous solution, Corros. Sci. 43 (2001) 1953–1961. doi:10.1016/S0010-938X(00)00188-8.

[40] V.K. William Grips, H.C. Barshilia, V.E. Selvi, Kalavati, K.S. Rajam, Electrochemical behavior of single layer CrN, TiN, TiAlN coatings and nanolayered TiAlN/CrN multilayer coatings prepared by reactive direct current magnetron sputtering, Thin Solid Films. 514 (2006) 204–211. doi:10.1016/j.tsf.2006.03.008.

[41] V.F. Lvovich, Impedance Spectroscopy: Applications to Electrochemical and Dielectric Phenomena, John Wiley & Sons, Inc., 2012. doi:10.1002/9781118164075.

[42] C. Liu, Q. Bi, A. Leyland, A. Matthews, An electrochemical impedance spectroscopy study of the corrosion behaviour of PVD coated steels in 0.5 N NaCl aqueous solution: Part II.: EIS interpretation of corrosion behaviour, Corros. Sci. 45 (2003) 1257–1273. doi:10.1016/S0010-938X(02)00214-7.

[43] K. Wu, W.S. Jung, J.W. Byeon, In-situ monitoring of pitting corrosion on vertically positioned 304 stainless steel by analyzing acoustic-emission energy parameter, Corros. Sci. 105 (2016) 8–16. doi: 10.1016/j.corsci.2015.12.010.

Figure Captions

Figure 1. SEM images of TiAlN coatings a) DC- produced with -40 V DC bias b) DP500-produced with superimposing -500 V pulse voltage on -40 V DC bias c) DP1000 produced with superimposing -1000 V pulse voltage on -40 V DC bias

Figure 2. Nyquist plots of steel substrate and TiAlN coated steels in deaerated 0.1 N HCl solution after 5 h immersion time. In this figure solid lines represent the fitted curves.

Figure 3. Equivalent circuit models; (a) generalized model for mild steel, (b) model for TiAlN coated steels.

Figure 4. Macro images of coated samples after ferroxyl test. (a) DC, (b) DP500, (c) DP1000.

Figure 5. SEM image of the corrosion site on the DC TiAlN coated steel. White circle indicates the trace of corroded substrate below the coating

Figure 6. SEM images of corroded sites determined by ferroxyl test after removal of their cap by ultrasonication. Arrows on the figures represent direction of gravity (a) DC, (b) DP500, (c) DP1000.

Figure 7. 2D and 3D optical profilometry images of the corroded sites of TiAlN coated samples after removal of their caps by ultrasonication. White arrows indicate the exemplar-corroded sites. (a) DC, (b) DP500, (c) DP1000.

Table 1. TiAlN coating parameters and thickness of the coatings.

Sample	Step	DC bias (V)	Pulse bias (V)-duty cycle (%)	Deposition temperature (ºC)	Coating thickness (µm)
DC	Ion etching Ti/TiN interlayer TiAlN coating	- -150 -40	-1000/80 % - -	285 ± 5	3.8
DP500	Ion etching Ti/TiN interlayer TiAlN coating	- -150 -40	-1000/80 % - -500/14 %	315 ± 15	3.6
DP1000	Ion etching Ti/TiN interlayer TiAlN coating	- -150 -40	-1000/80 % - -1000/14 %	400 ± 30	3.9

Table 2. R_p of uncoated and TiAlN coated steel depending on immersion time in 0.1N HCl solution.

Immersion time (min)	**Mild steel R_{p1} (ohm.cm^2)**	**DC R_{p2} (ohm.cm^2)**	**DP500 R_{p3} (ohm.cm^2)**	**DP1000 R_{p4} (ohm.cm^2)**
50	1751	5936	6284	16456
130	1367	3500	4168	11643
210	1241	2249	4042	9479
290	1159	1601	3314	6683

Table 3. EIS fitting results of the samples (after 5 h exposure to 0.1 N HCl).

	R_s (ohm)	Q_{dl}*10^{-2} (µF.s^{n-1}.cm^{-2})	n_{dl}	R_p (ohm.cm^2)	R_{pore} (ohm.cm^2)	Q_{coat}*10^{-2} (µF.s^{n-1}.cm^{-2})	n_{coat}
Steel	10	22.5	0.73	1132	-	-	-
DC	16	10	0.70	1535	60	40	0.84
DP500	15	3.75	0.68	3120	120	18	0.90
DP1000	14	3.13	0.65	6240	240	16	0.91

Table 4. Numbers of defect sites in the coatings that were determined with ferroxyl test after 5 h exposure to 0.1 N HCl solution

	DC	DP500	DP1000
Number of defects/cm^2	38	25	2

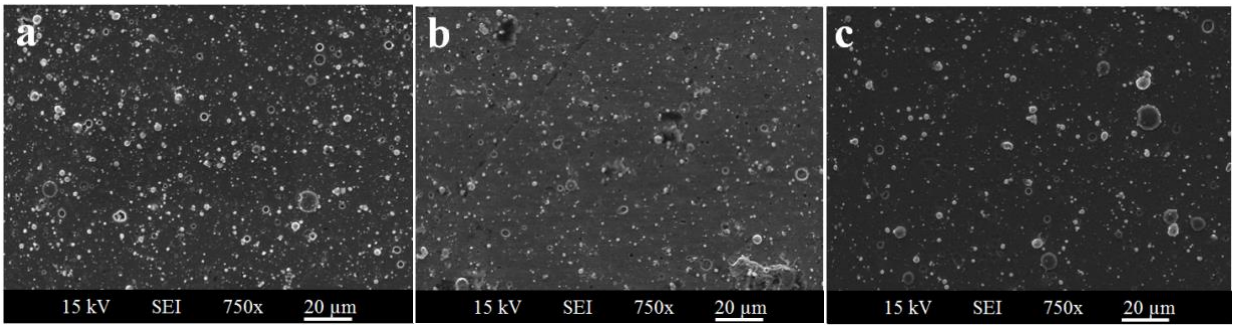

Figure 1

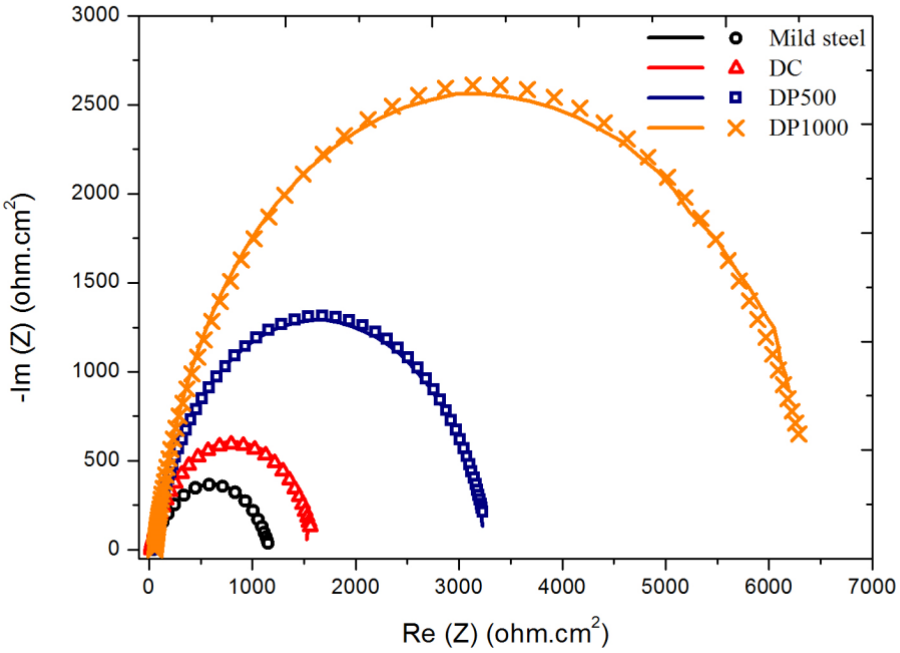

Figure 2

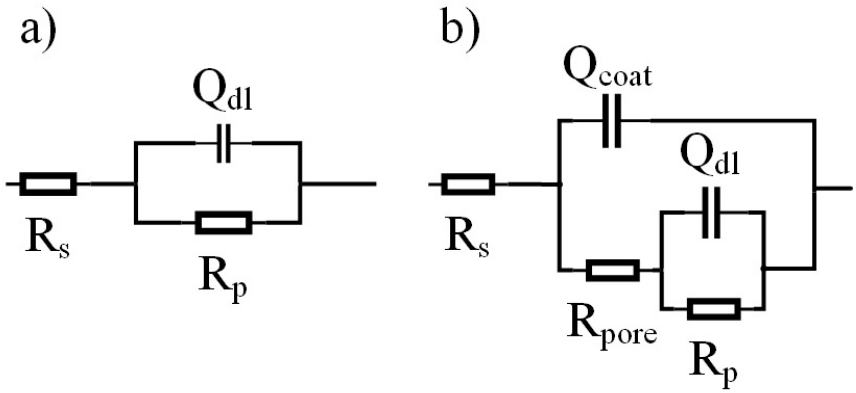

Figure 3

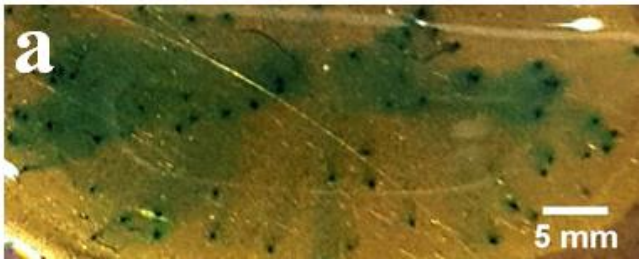

Figure 4a

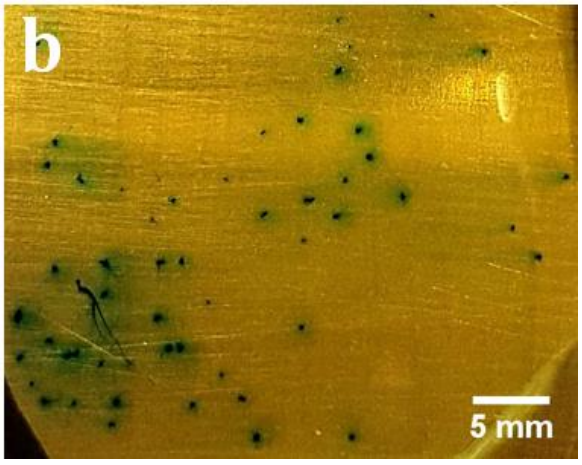

Figure 4b

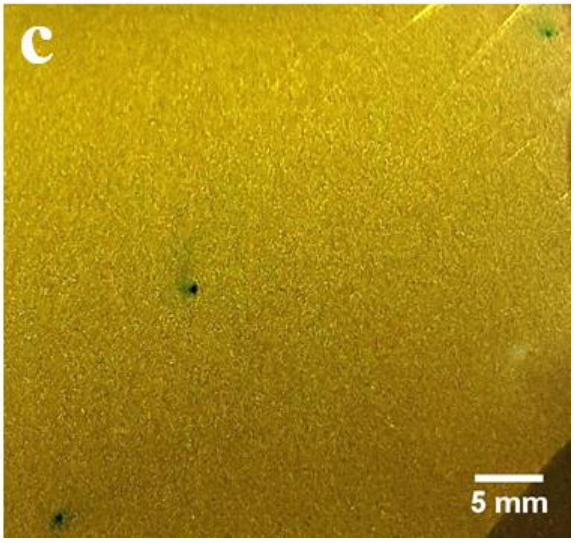

Figure 4c

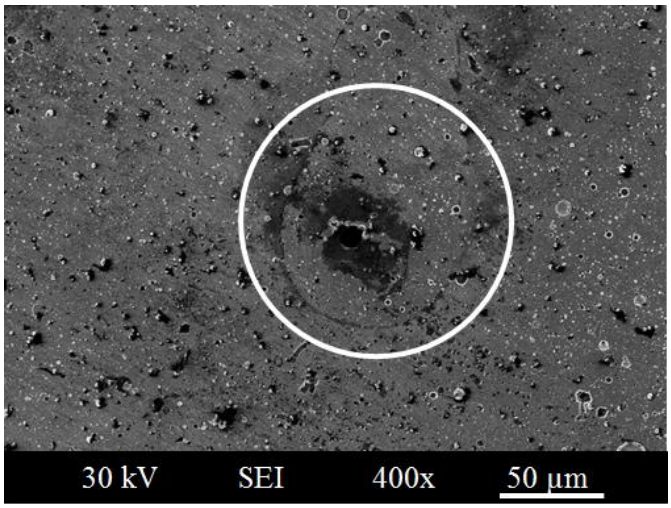

Figure 5.

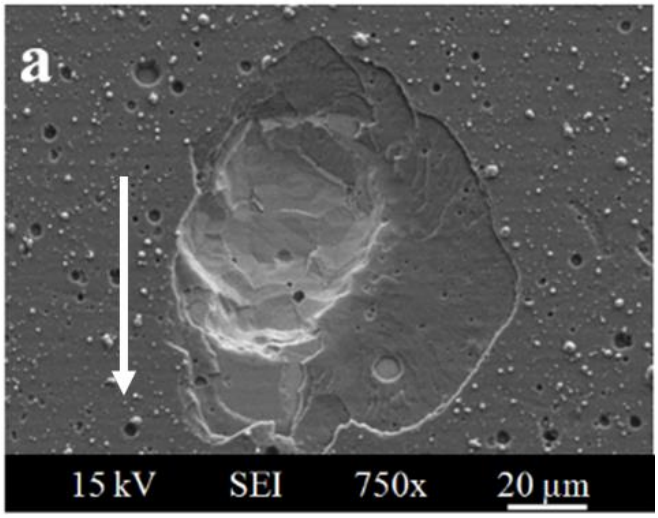

Figure 6a

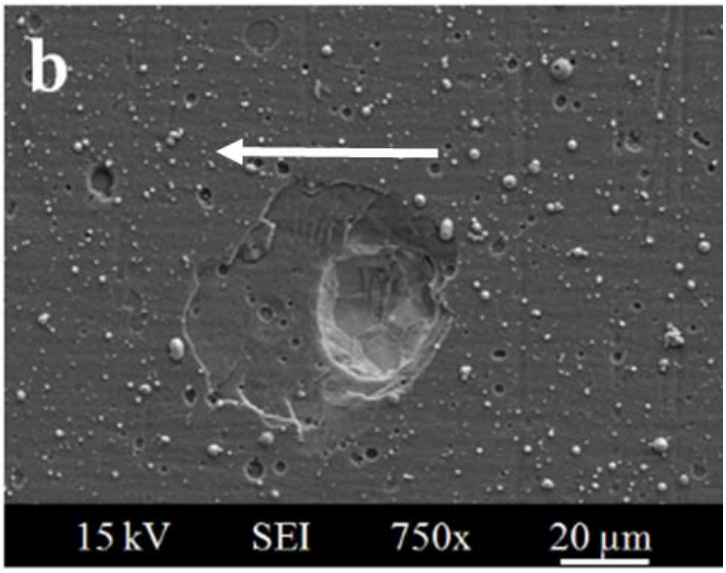

Figure 6b

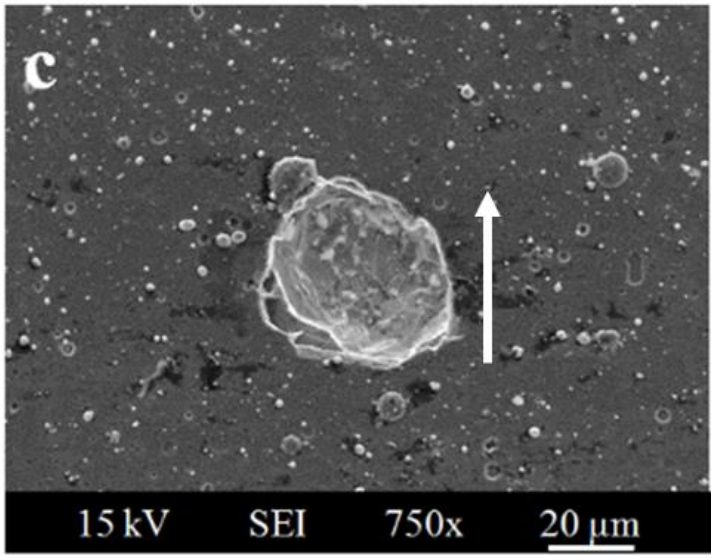

Figure 6c

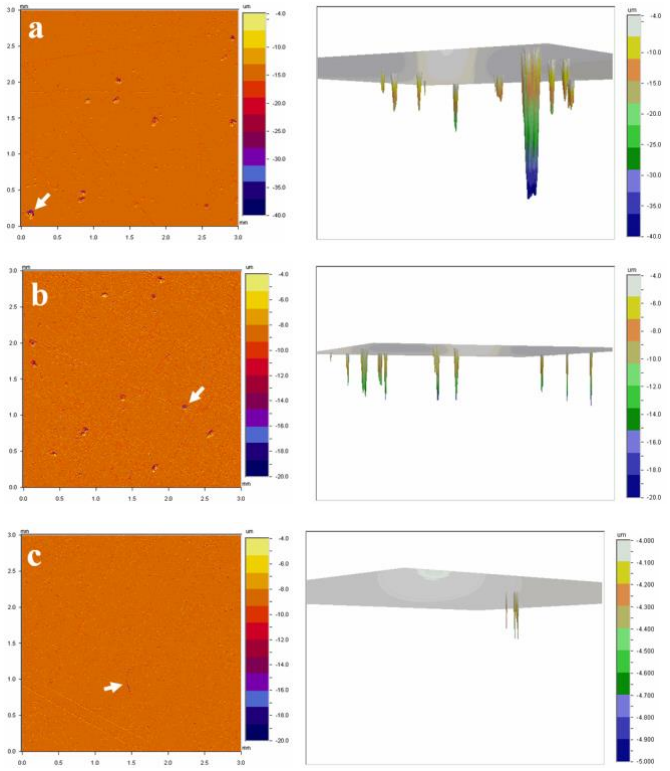

Figure 7